

Analysis on the Rock–Cutter Interaction Mechanism During the TBM Tunneling Process

Haiqing Yang^{1,2} · He Wang¹ · Xiaoping Zhou¹

Received: 14 November 2014 / Accepted: 11 July 2015 / Published online: 21 July 2015
© Springer-Verlag Wien 2015

Abstract The accurate prediction of rock cutting forces of disc cutters is crucial for tunnel boring machine (TBM) design and construction. Disc cutter wear, which affects TBM penetration performance, has frequently been found at TBM sites. By considering the operating path and wear of the disc cutter, a new model is proposed for evaluating the cutting force and wear of the disc cutter in the tunneling process. The circular path adopted herein, which is the actual running path of the TBM disc cutter, shows that the lateral force of the disc cutter is asymmetric. The lateral forces on the sides of the disc cutter are clearly different. However, traditional solutions are obtained by assuming a linear path, where the lateral forces are viewed as equal. To simulate the interaction between the rock and disc cutter, a simple brittle damage model for rock mass is introduced here. Based on the explicit dynamic finite element method, the cutting force acting on the rock generated by a single disc cutter is simulated. It is shown that the lateral cutting force of the disc cutter strongly affects the wear extent of disc cutter. The wear mechanism is thus underestimated by the classical model, which was obtained by linear cutting tests. The simulation results are discussed and compared with other models, and these simulation results agree well with the results of present ones.

Keywords Wear · Cutting force · TBM · Numerical modeling · Disc cutter

Abbreviations

D	Damage tensor
E_{ij}	Undamaged elastic tensor
σ	Stress second-order tensors
D₁, D₂, D₃	Three principal damage components
E, G	Elastic modulus and shear modulus
F	Vertical force acting on disc cutter
F_n	Normal force
F_r	Rolling force
F_{np}, F_{rp}	Path correction terms
F_{nw}, F_{rw}	Wear correction terms
F_{np}	Average normal force acting on the disc cutter
F_{si}, F_{so}	Inner lateral force and outer lateral force
I	Wear rate of energy
L	Boring distance
M	Abrasive volume of the disc cutter
M'	Cutter radial wear extent
N	Number of revolutions per minute of the TBM
R	Disc cutter radius
R'	Installing radius of the disc cutter
S	Contact area
T	Cutter tip width
V	Tangential velocity of the disc cutter
V₀	Tunneling velocity of the cutter head
W	Friction power
a, b	Normal contact stress coefficients
f_{max}	Maximum contact stress
h	Penetration depth
k_{np}, k_{rp}	Rock fragment path correction coefficients
k_{nw}, k_{rw}	Wear coefficients
l	Full arc length
m	Number of disc cutters used on the cutter head

✉ Haiqing Yang
yanghaiqing06@163.com

¹ School of Civil Engineering, Chongqing University, Chongqing, China

² Key Laboratory of Transportation Tunnel Engineering, Ministry of Education, Chengdu 610031, China

n	Parameter characterizing the material brittleness
p	Cutter penetration depth
t	Boring time
w_1, w_2	Angular rotation and revolution velocities of disc cutter
μ	Friction coefficient
ϕ	Angle of the theoretical contact arc
ξ	Slip ratio
$\varepsilon_1, \varepsilon_2, \varepsilon_3$	Principal strain components
ε_c	Allowable tensile strain
λ	Lame constant
ν	Poisson's ratio
σ_c	Rock uniaxial compressive strength
α	Edge angle of the disc cutter

1 Introduction

Tunnel boring machines (TBM) play an increasingly important role in hard rock tunnel excavation. For example, they were widely adopted in two deep tunnels in Jinping II hydropower station, China (Li et al. 2012); In the process of rock breakage, the performance of the cutter directly influences the work efficiency of the TBM. Most of the calculation models for cutting forces are based on linear path tests, while the running paths of cutter in engineering applications are circular. This incompatibility may lead to large errors, which may in turn cause engineering damage.

During tunnel boring machine (TBM) excavation, TBM cutters roll across the tunnel face and continuously expand the crushed zone immediately below. Cracks then initiate from the crushed zone and propagate downwards and to the side. Under the action of the rolling cutter, one or more cracks may reach the free surface or propagate to meet the cracks of the neighboring cuts. In these two cases, chipping occurs. The first case, wherein the cracks reach the free surface, is similar to the chip formation of a single cutter indentation process. This process has been extensively studied via numerical simulations and experiments (Cook et al. 1984; Pang and Goldsmith 1990; Chiaia 2001; Liu et al. 2002; Gong and Zhao 2005). The latter case, wherein cracks propagate to meet the cracks of neighboring cuts, involves the interaction between two adjacent cuts and is directly relevant to the design of TBM cutter heads and TBM excavation efficiency.

Currently, single disc cutters are the most commonly used roller cutters for hard rock TBM because of their highly efficient rock mass damage capabilities. Their geometry and wear characteristics have significant effects on the efficiency of energy transfer to the rock and the

maximum penetration rate (Cigla et al. 2001). The wear extent of disc cutter can be defined as the difference between the original radius of the disc cutter and its radius after operation (Rad 1975; Liu 2003; Wan et al. 2002). When the wear extent exceeds a certain length, the disc cutter is no longer effective for cutting rock. Statistically, the dissipative expenditure of the cutter is at least one fifth of the project cost, and the time spent replacing the cutter accounts for almost one third of the total project time (Su et al. 2010). Consequently, the effect of the disc cutter wear condition on rock breakage is an important topic for improving TBM working performance. One of the major current research trends is the search for new technologies to assist and improve TBM design. The present work focuses on the numerical simulation of rock breakage by a disc cutter using the explicit dynamic finite element method (FEM) ANSYS/LS DYNA. This numerical technique is used to establish a method of estimating the disc cutter cutting force by considering the effects of the running path and wear of the disc cutter.

Numerical modeling methods have been adopted to investigate the mechanism of TBM rock fragmentation. Numerical models able to accurately simulate the process of rock fragmentation would facilitate the assessment of the performance of TBMs. Cook et al. (1984) compared the results of a numerical simulation (using a 2D FEM model) with the experimental results for rock fragmentation induced by an indenter. Bilgin et al. (2000) employed Franc2D/L (2D linear elastic FEM software) to investigate the effect of lateral stress on the cutting efficiency of two materials (plaster and concrete) using chisel-type cutters. Liu et al. (2002) and Kou et al. (2004) used the rock–tool interaction code R-T^{2D} to model the rock fragmentation process induced by single and double indenters. This model accommodates heterogeneous rock properties, and dynamic cracking patterns were observed too. Baek and Moon (2003) employed a heterogeneous model using the finite difference method (FDM) to analyze the influence of confining pressure and cutter spacing on the chipping mechanism of rock. (Gong and Zhao 2005, Gong et al. 2006) studied the effect of joint spacing and orientation on rock fragmentation using the 2D discrete element method (DEM) based on Universal Distinct Element Code (UDEC).

Previous work on disc cutter wear prediction can be divided into two categories. The first category involves the development of a formula or rule to predict disc cutter wear based on the TBM working parameters. For example, Zhang (2006) developed a method to estimate cutter wear by analyzing tunneling parameters. Based on a single factor mechanical model of a disc cutter, an Empirical formula was established to predict cutter wear condition. Zhao et al. (2007) fitted the interactive rules between the field

penetration index and cutting coefficient with different boring performances according to on-site Qinling tunnel boring data. The interactive rules could be used to identify abnormal cutter wear. The second category of disc cutter wear prediction studies utilizes a parameter to denote the abrasion characteristics of the disc cutters as they cut into rock masses. For example, Zhang and Ji (2009) introduced the concept of an arc length wear-out coefficient to calculate the disc cutter wear extent. The Colorado School of Mines (CSM) model for TBM performance prediction, developed by the Earth Mechanics Institute, estimates the cutter life in terms of the Cerchar abrasivity index (CAI). The Norwegian Institute of Technology (NTU) model uses a specialized abrasiveness value (AV) to estimate cutter life (Rostami et al. 1996).

Clearly, the aforementioned prediction methods are mostly based on an empirical or semi-theoretical equation, a fitted rule, or a testing approach. Earlier studies ignore the change in disc cutter performance resulting from cutter wear and the operating path of rock breakage. In this paper, based on the assumption of a contact pressure distribution between the cutter ring and rock, the path correction coefficient is introduced to amend the cutting force. Likewise, the wear correction coefficient is also introduced to amend the cutting force. Next, a theoretical model that includes the disc cutter operating path and wear in the boring process is proposed to estimate the cutting force by incorporating the appropriate correction terms. The cutting force acting on the rock is simulated by the explicit dynamic finite element method (FEM), and the damage field of rock breakage is also obtained. The results obtained via published methods (Roxborough and Phillips 1975; Evans and Pomeroy 1966; Zhang 2008), via numerical simulation and via the present model are compared.

We intend to describe a new model for evaluating the cutting force and wear of the disc cutter during the tunneling process. In Sect. 2, a new formula for the cutting forces that accounts for both the actual operating path of the disc cutter and the disc cutter wear is derived. In Sect. 3, a model for predicting the disc cutter wear extent is proposed, and the effects of the boring parameters on the wear extent are discussed. In Sect. 4, the numerical simulation model of the cutting process is analyzed in detail. Finally, the results obtained via published methods, via numerical simulation and via the present model are compared to illustrate the validity of the present model.

2 Mechanism of the Rock Fragmenting Process by Disc Cutters

In the TBM tunneling process, the disc cutter is the primary rock cutting tool and is subjected to high cutting loads. The disc cutter is the main wearing part of the TBM, and its

performance directly affects the efficiency of the TBM and the tunnel excavation progress. Therefore, studies on the mechanism of the rock fragmenting process by disc cutters and the cutting forces acting on disc cutters are highly significant for the prediction of the excavation performance of the entire TBM. In the following study, a new formula for calculating cutting forces while disc cutter wear is considered is derived.

2.1 Cutting Force Acting on the TBM Disc Cutter

Estimating the forces for cutting a certain type of rock with a disc cutter is an essential aspect of TBM cutter head design and performance prediction. The estimated cutting forces can be utilized for many purposes, and their accuracy depends on the level of understanding of the cutting process.

In early studies, the contact zone or contact area between the disc cutter and rock surface was estimated based on classical theories and the cutting geometry shown in Fig. 1. This figure presents the generalized pressure distribution within the contact area based on the cutting geometry, including the disc diameter and depth of penetration.

As shown in Fig. 1, R is the disc cutter radius, ϕ is the angle of the theoretical contact arc, and p is the cutter penetration depth. The relationship between the depth of cutter penetration, disc cutter radius and angle of the theoretical contact arc can be expressed simply as

$$p = R(1 - \cos \phi) \quad (1)$$

Based on the distribution model of normal contact stress along the long parabolic type contact arc (Yu and Qian 1990) at the interface between the cutting tool and rock mass, the parabolic equation for the stress distribution can be defined as follows (Yu and Qian 1990; Liu et al. 2013):

$$f(x) = ax^2 + bx \quad (2)$$

where $f(x)$ is the normal contact stress of an arbitrary point on the contact arc; x is the corresponding arc length; and a and b are undetermined coefficients. Substituting the corresponding arc length x , we have

$$f(\theta) = aR^2\theta^2 + bR\theta \quad (3)$$

The parabolic law shows that $x = 0$, $\theta = 0$, $f(x) = 0$; $x = l$, $\theta = \phi$, $f(l) = 0$; $x = l/2$, $\theta = \phi/2$, and $f(l/2) = f_{\max}$ where l is the full arc length, ϕ is the angle of the full contact arc in radians, and f_{\max} is the maximum contact stress. We obtain the parabolic equation of the normal contact stress distribution:

$$f(\theta) = 4f_{\max} \frac{\theta}{\phi} \left(1 - \frac{\theta}{\phi} \right) \quad (4)$$

The force acting on an arbitrary infinitesimal of the contact arc can then be expressed as

$$dF = 4f_{\max} \frac{\theta}{\phi} \left(1 - \frac{\theta}{\phi}\right) \cdot dS = 4f_{\max} \frac{\theta}{\phi} \left(1 - \frac{\theta}{\phi}\right) \cdot TRd\theta$$

$$= 4f_{\max} TR \frac{\theta}{\phi} \left(1 - \frac{\theta}{\phi}\right) d\theta \tag{5}$$

where S is the contact area and T is the tip width. The normal force F_n and rolling force F_r components of the disc cutter cutting force can be expressed as follows:

$$F_n = \int_0^\phi dF \cos \theta = \int_0^\phi 4f_{\max} TR \frac{\theta}{\phi} \left(1 - \frac{\theta}{\phi}\right) \cos \theta d\theta$$

$$= \frac{4f_{\max} TR}{\phi} \left(\frac{2 \sin \phi}{\phi} - \cos \phi - 1\right) \tag{6}$$

$$F_r = \int_0^\phi dF \sin \theta = \int_0^\phi 4f_{\max} TR \frac{\theta}{\phi} \left(1 - \frac{\theta}{\phi}\right) \sin \theta d\theta$$

$$= \frac{4f_{\max} TR}{\phi} \left(\frac{2 - 2 \cos \phi}{\phi} - \sin \phi\right) \tag{7}$$

In the above expression of the normal force F_n and rolling force F_r , only the maximum normal contact stress associated with rock mass parameters is considered. Substituting Eq. (1) into Eqs. (6) and (7), the relationship between the normal force F_n and penetration p and the relationship between the rolling force F_r and penetration p can be obtained as

$$F_n = \frac{4f_{\max} T}{\arccos(1 - p/R)} \left(\frac{2\sqrt{R^2 - (R - p)^2}}{\arccos(1 - p/R)} + p - 2R\right) \tag{8}$$

$$F_r = \frac{4f_{\max} T}{\arccos(1 - p/R)} \left(\frac{2p}{\arccos(1 - p/R)} - \sqrt{R^2 - (R - p)^2}\right) \tag{9}$$

Under actual operation, the disc cutter operating path for rock breaking is an arc, and rock breaking induces wear in the disc cutter. In most studies (Paul and Sikarskie 1965; Roxborough and Phillips 1975), the forces on the two sides of the disc cutter generated by surrounding rock are treated as equal, i.e., $F_2 = F_3$, which suggests that the lateral force acting on the disc cutter is equal to zero, i.e., $F_{si} = F_{so}$. Meanwhile, in actual cutting processes, the disc cutter operating path for rock breaking is an arc, and the shear bodies on the two sides of the disc cutter differ. As a result, rock failure on each side does not occur simultaneously, and the lateral forces on the sides of the disc cutter are clearly different $F_{si} \neq F_{so}$. This phenomenon also inevitably leads to variation in the normal and rolling forces, which affects the cutter’s performance. To address this issue, we introduce a correction to improve the rock breakage efficiency.

Based on the above analysis, we introduce the rock fragment path correction coefficients k_{np} and k_{rp} . The correction terms F_{np} and F_{rp} can then be expressed as follows:

$$F_{np} = k_{np} \frac{4f_{\max} T}{\arccos(1 - p/R)} \left(\frac{2\sqrt{R^2 - (R - p)^2}}{\arccos(1 - p/R)} + p - 2R\right) \tag{10}$$

$$F_{rp} = k_{rp} \frac{4f_{\max} T}{\arccos(1 - p/R)} \left(\frac{2p}{\arccos(1 - p/R)} - \sqrt{R^2 - (R - p)^2}\right) \tag{11}$$

From the analysis above, in the actual rock breakage process, the lateral forces acting on the inner and outer cutter ring are unequal, i.e., $F_{si} \neq F_{so}$. Thus, the relationship between the lateral force on both sides of the cutter and the normal force can be expressed as follows (based on a large number of numerical tests).

$$F_{si} = -12.84 + 92.77e^{-m^{0.72}} \cdot \sin[(m - 0.04)/0.167] \tag{12}$$

$$F_{so} = -0.063 + 20.422e^{-\frac{1}{m^{6.33}}} \cdot \sin[(m - 0.336)/0.132] \tag{13}$$

where $m = 0.0942 \arcsin \frac{F_{np} - \bar{F}_{np}}{41.823} + 0.17$, F_{np} is the normal force acting on the disc cutter, \bar{F}_{np} is the average normal force acting on the disc cutter, F_{si} is the inner lateral force, and F_{so} is the outer lateral force.

From a contact mechanics perspective, roll is the relative motion of two objects in contact around the axis parallel to a common tangent plane. Meanwhile, slip is the relative displacement of the contact point between two surfaces. It is clear that roll and slip are likely to exist simultaneously. According to the relationship between elastic deformation and friction, the contact area can be divided into glue and slip zones, as shown in Fig. 1.

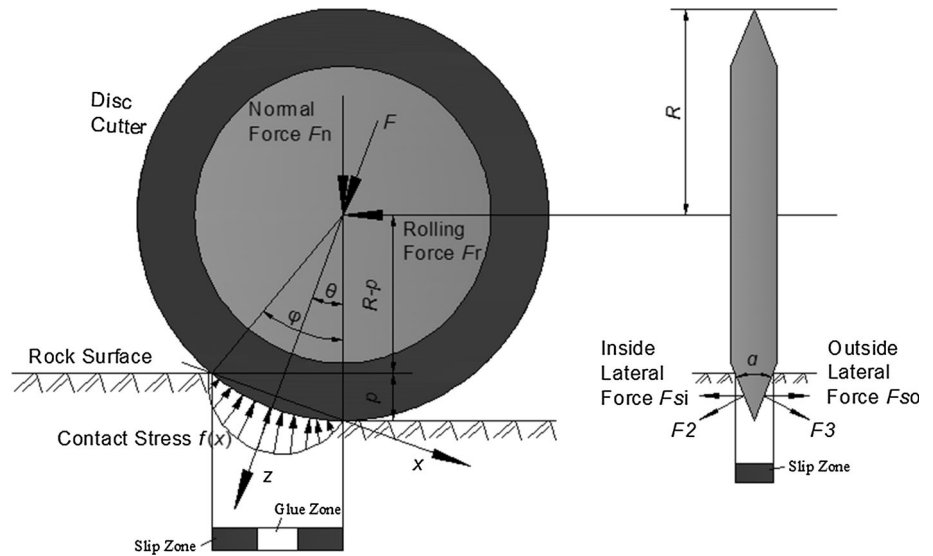
Under the partial slip condition, if the tangential force increases to the limit of the friction force μF , the objects have a sliding moment, and the contact zone width is $2a$, the tangential force can be expressed as follows based on the friction law (Goryacheva and Goryachev 2006):

$$T'(x) = \mu F(x) = \frac{2\mu F}{a\pi} \left(1 - \frac{x^2}{a^2}\right)^{\frac{1}{2}} \tag{14}$$

When the tangential force is below the critical friction force μF , a glue zone is present in the center of the contact region. Setting the glue zone width as c , the additional force distribution in the glue zone can be expressed as

$$T''(x) = -\frac{c}{a} \frac{2\mu F}{a\pi} \left(1 - \frac{x^2}{a^2}\right)^{\frac{1}{2}} \tag{15}$$

Fig. 1 Generalized illustration of the contact area between a single disc cutter and rock



The tangential force can then be obtained by Eqs. (14) and (15) as

$$T(x) = T'(x) + T''(x) = \frac{2\mu F}{a^2\pi} \left[(a^2 - x^2)^{\frac{1}{2}} - (c^2 - x^2)^{\frac{1}{2}} \right] \tag{16}$$

and the total tangential force acting on the contact surface can be determined as

$$Q = \int_{-a}^a T(x) dx = \int_{-a}^a T'(x) dx + \int_{-c}^c T''(x) dx = \mu F - \frac{c^2}{a^2} \mu F \tag{17}$$

where F is the normal force of the disc cutter, Q is the rolling force of the disc cutter, and μ is the friction coefficient.

The slip ratio of rolling objects is the ratio of the sliding distance to the total rolling distance. Therefore, the slip ratio ξ and slip speed S can be calculated according to contact theory as follows (Tohnson 1989):

$$\xi = \frac{\mu a}{R} \left[1 - \left(1 - \frac{Q}{\mu F} \right)^{\frac{1}{2}} \right] \tag{18}$$

$$S = \xi V \tag{19}$$

where V is the tangential velocity of the disc cutter, which can be calculated by $V = 2\pi R'N$, $V = 2\pi R'N$. Here, R' is the distance between the center of the cutter head and the disc cutter, i.e., the installing radius of the disc cutter, and N is the number of revolutions per minute of the TBM.

According to the principle of friction, the sliding friction power is the product of the friction force and the sliding distance. The friction power W can then be expressed as follows:

$$W = \mu F S t \tag{20}$$

where μ is the friction coefficient; t is the boring time, which can be calculated by $t = L/LV_0$; L is the boring distance; V_0 is the tunneling velocity of the cutter head, $V_0 = pmN$; and m is the number of disc cutters used on the cutter head for a given R' .

According to Roxborough FF's estimating formula (Roxborough and Phillips 1975), the relationship between the normal force F and rolling force Q is

$$\frac{Q}{F} = \sqrt{\frac{p}{2R - p}} \tag{21}$$

By substituting Eqs. (18) and (19) into (20), the friction power W can be expressed as follows:

$$W = \mu F V t \left[\frac{\mu a}{R} \left[1 - \left(1 - \frac{Q}{\mu F} \right)^{\frac{1}{2}} \right] \right] \tag{22}$$

A proportional relationship between the abrasive volume of the disc cutter and the friction power was assumed, with the proportionality being related to the material properties. The wear rate of energy I was introduced as the proportional relationship between the abrasive volume of the disc cutter and the friction power. The wear rate of energy was defined as the abrasive volume of the disc cutter per unit of friction power under the experimental conditions. Therefore, the abrasive volume of the disc cutter M in the tunneling process can be expressed as follows (Li et al. 2011):

$$M = IW \tag{23}$$

where I is the wear rate of energy and W is the friction power.

By substituting Eqs. (22) into (23),

$$\frac{M}{I} = \mu F V t \left[\frac{\mu a}{R} \left[1 - \left(1 - \frac{Q}{\mu F} \right)^{\frac{1}{2}} \right] \right] \tag{24}$$

The normal force F_n can then be obtained by Eq. (24) as follows:

$$F_n = \frac{M V_0}{\mu^2 \phi \pi R' N I L} \cdot \frac{1}{1 - \sqrt{1 - \frac{1}{\mu} \sqrt{\frac{p}{2R-p}}}} \tag{25}$$

According to Eq. (21), the rolling force of the disc cutter can be determined as follows:

$$F_r = \frac{M V_0}{\mu^2 \phi \pi R' N I L} \cdot \frac{\sqrt{\frac{p}{2R-p}}}{1 - \sqrt{1 - \frac{1}{\mu} \sqrt{\frac{p}{2R-p}}}} \tag{26}$$

Considering the effect of cutting tool wear on the normal force and the rolling force, we introduce the wear coefficients k_{nw} and k_{rw} . The wear correction term can then be expressed as follows:

$$F_{nw} = k_{nw} \frac{M V_0}{\mu^2 \phi \pi R' N I L} \cdot \frac{1}{1 - \sqrt{1 - \frac{1}{\mu} \sqrt{\frac{p}{2R-p}}}} \tag{27}$$

$$F_{rw} = k_{rw} \frac{M V_0}{\mu^2 \phi \pi R' N I L} \cdot \frac{\sqrt{\frac{p}{2R-p}}}{1 - \sqrt{1 - \frac{1}{\mu} \sqrt{\frac{p}{2R-p}}}} \tag{28}$$

where M is the bulk wear extent, which can be translated into the radial wear extent according to the disc cutter structural parameters; k_{nw} and k_{rw} are the wear correction coefficients; and R is the disc cutter radius.

Therefore, considering the effects of the disc cutter path and wear, the normal and rolling forces can be expressed as follows:

$$\begin{aligned} F_n &= F_{np} + F_{nw} \\ &= k_{np} \frac{4f_{\max} T}{\arccos(1-p/R)} \left(\frac{2\sqrt{R^2 - (R-p)^2}}{\arccos(1-p/R)} + p - 2R \right) \\ &\quad + k_{nw} \frac{M V_0}{\mu^2 \arccos(1-p/R) \pi R' N I L} \cdot \frac{1}{1 - \sqrt{1 - \frac{1}{\mu} \sqrt{\frac{p}{2R-p}}}} \end{aligned} \tag{29}$$

$$\begin{aligned} F_r &= F_{rp} + F_{rw} = k_{rp} \frac{4f_{\max} T}{\arccos(1-p/R)} \\ &\quad \times \left(\frac{2p}{\arccos(1-p/R)} - \sqrt{R^2 - (R-p)^2} \right) \\ &\quad + k_{rw} \frac{M V_0}{\mu^2 \arccos(1-p/R) \pi R' N I L} \cdot \frac{\sqrt{\frac{p}{2R-p}}}{1 - \sqrt{1 - \frac{1}{\mu} \sqrt{\frac{p}{2R-p}}}} \end{aligned} \tag{30}$$

By substituting Eqs. (29) and (30) into Eqs. (12) and (13), respectively, the lateral force acting on each side of the disc cutter can be expressed as follows:

$$F_{si} = -12.84 + 92.77 e^{-m^{0.72}} \cdot \sin[(m - 0.04)/0.167] \tag{31}$$

$$F_{so} = -0.063 + 20.422 e^{-\frac{1}{m^{6.33}}} \cdot \sin[(m - 0.336)/0.132] \tag{32}$$

where $m = 0.0942 \arcsin \frac{F_n - \bar{F}_n}{41.823} + 0.17$, F_n is the normal force, and \bar{F}_n is the average normal force of the disc cutter.

2.2 Damage to Rock Caused by the Disc Cutter

Fractures were observed directly by digital optical televiewer during TBM construction, they exist ahead of TBM face and tunnel sidewall, and the affected range is about two times and 0.22-times tunnel diameter, respectively (Li et al. 2012, 2013).

In this paper, the damage tensor is established based on the strain state of the material (Zhang and Lu 2010), and the damage evolution equation is derived according to the elastic brittle constitutive relation and the corresponding yield criterion to study damage to rock under the action of the disc cutter.

2.2.1 Damage Variable and Damage Evolution Equation

Previous studies have shown that concrete material damage during uniaxial compression is caused by tensile stress and that the damage direction is orthogonal to the loading direction, which indicates that the concrete damage is anisotropic or orthotropic (Yu and Qian 1990). The properties of hard rock are similar to those of the concrete material, and rock material can be considered orthotropic. In the principal stress space, it is

assumed that the principle stress and the principle damage axis coincide. The initial state of the material is an isotropic linear elastic body, and the orthotropic property was observed after damage. According to this assumption, the damage tensor \mathbf{D} and the stress tensor $\boldsymbol{\sigma}$ are second-order tensors. Suppose D_1 , D_2 and D_3 are three principal damage components. According to the second law of thermodynamics and the physical meaning of a damage variable, the damage variable can be expressed as (Zhang and Lu 2010)

$$\begin{cases} D_1 = \frac{1}{2} \left[\left[\frac{\langle \varepsilon_1 \rangle}{\varepsilon_c} \right]^n + \left[v \frac{\langle \varepsilon_2 \rangle}{\varepsilon_c} \right]^n + \left[v \frac{\langle \varepsilon_3 \rangle}{\varepsilon_c} \right]^n \right] \\ D_2 = \frac{1}{2} \left[\left[v \frac{\langle \varepsilon_1 \rangle}{\varepsilon_c} \right]^n + \left[\frac{\langle \varepsilon_2 \rangle}{\varepsilon_c} \right]^n + \left[v \frac{\langle \varepsilon_3 \rangle}{\varepsilon_c} \right]^n \right] \\ D_3 = \frac{1}{2} \left[\left[v \frac{\langle \varepsilon_1 \rangle}{\varepsilon_c} \right]^n + \left[v \frac{\langle \varepsilon_2 \rangle}{\varepsilon_c} \right]^n + \left[\frac{\langle \varepsilon_3 \rangle}{\varepsilon_c} \right]^n \right] \end{cases} \quad (33)$$

where $\langle x \rangle = (|x| - x)/2$; v is Poisson’s ratio; ε_1 , ε_2 , and ε_3 are the principal strain components; and ε_c is the allowable tensile strain. At $\varepsilon = \varepsilon_c$, the material is destroyed. ε_c is obtained as the limit of the tensile strain in uniaxial tensile tests. Finally, n is a parameter characterizing the material brittleness, with larger values corresponding to greater brittleness.

In uniaxial compression ($\sigma_1 > 0$, $\sigma_2 = \sigma_3 = 0$), $\varepsilon_1 > 0$, $\varepsilon_2 = \varepsilon_3 = \varepsilon'$, and $\varepsilon' < 0$. Thus, Eq. (33) becomes

$$\begin{cases} D_1 = \frac{1}{2} \left[\left[v \frac{\varepsilon'}{\varepsilon_c} \right]^n + \left[v \frac{\varepsilon'}{\varepsilon_c} \right]^n \right] \\ D_2 = \frac{1}{2} \left[\left[v \frac{\varepsilon'}{\varepsilon_c} \right]^n + \left[\frac{\varepsilon'}{\varepsilon_c} \right]^n \right] \\ D_3 = \frac{1}{2} \left[\left[\frac{\varepsilon'}{\varepsilon_c} \right]^n + \left[v \frac{\varepsilon'}{\varepsilon_c} \right]^n \right] \end{cases} \quad (34)$$

The direction of the specimen damage is generally consistent with the direction of compressive stress in the same direction, which can be observed in rock specimen uniaxial compression tests. This also coincides with Eq. (34), where $D_1 < D_2 = D_3$. In addition, according to Eq. (34), damage also emerges in the σ_3 direction. Because the microcrack’s direction is not completely consistent with the macroscopic crack direction during failure, the direction of initial microcracks are somewhat random, which is the meaning of D_1 .

2.2.2 Elastic-Brittle Material Damage Constitutive Equation

The flexibility matrix of the undamaged condition is as follows:

$$E_{ij} = \begin{bmatrix} \lambda + 2G & \lambda & \lambda \\ \lambda & \lambda + 2G & \lambda \\ \lambda & \lambda & \lambda + 2G \end{bmatrix} \quad (35)$$

where λ and G are the Lamé constant and shear modulus, respectively.

Therefore, in the principal stress direction,

$$\sigma = (\lambda + 2G)\varepsilon \quad (36)$$

According to the principle of energy equivalence proposed by Sidoroff (An et al. 1991), for the damaged material, the flexibility tensor is

$$E_{ij} = (1 - D_i)^{1/2} E_{ij} (1 - D_j)^{1/2} \quad (37)$$

where E_{ij} is the undamaged elastic tensor. According to Eqs. (35) and (37),

$$E_{ij} = (\lambda + 2G\delta_{ij})(1 - D_i)^{1/2}(1 - D_j)^{1/2} \quad (38)$$

According to the generalized Hooke’s law and Eq. (38), the constitutive relations of elastic brittle damage can be expressed as

$$\begin{cases} \varepsilon_1 = \frac{\sigma_1}{E(1 - D_1)^2} - \frac{v\sigma_2}{E(1 - D_1)(1 - D_2)} - \frac{v\sigma_3}{E(1 - D_1)(1 - D_3)} \\ \varepsilon_2 = -\frac{v\sigma_1}{E(1 - D_1)(1 - D_2)} + \frac{\sigma_2}{E(1 - D_2)^2} - \frac{v\sigma_3}{E(1 - D_2)(1 - D_3)} \\ \varepsilon_3 = -\frac{v\sigma_1}{E(1 - D_1)(1 - D_3)} - \frac{v\sigma_2}{E(1 - D_2)(1 - D_3)} + \frac{\sigma_3}{E(1 - D_3)^2} \end{cases} \quad (39)$$

That is,

$$\{\varepsilon\} = \begin{bmatrix} \frac{1}{E(1 - D_1)^2} & -\frac{v}{E(1 - D_1)(1 - D_2)} & -\frac{v}{E(1 - D_1)(1 - D_3)} \\ -\frac{v}{E(1 - D_1)(1 - D_2)} & \frac{1}{E(1 - D_2)^2} & -\frac{v}{E(1 - D_2)(1 - D_3)} \\ -\frac{v}{E(1 - D_1)(1 - D_3)} & -\frac{v}{E(1 - D_2)(1 - D_3)} & \frac{1}{E(1 - D_3)^2} \end{bmatrix} \quad (40)$$

where σ_1 , σ_2 , and σ_3 are the principal stress components; ε_1 , ε_2 , and ε_3 are the principal strain components; and D_1 , D_2 , and D_3 are the damage components corresponding to the directions of three principal stresses. Finally, E is the elastic modulus. There are five independent components because $D_1 \neq D_2 \neq D_3$.

3 Analysis of the Abrasive Disc Cutter Wear During TBM Tunneling

In general, material wear is related to the sliding contact, and it may involve different mechanisms at various stages of the mechanical process. Material wear depends on the properties of the material surfaces, the surface roughness, the sliding distance, the sliding velocity and the

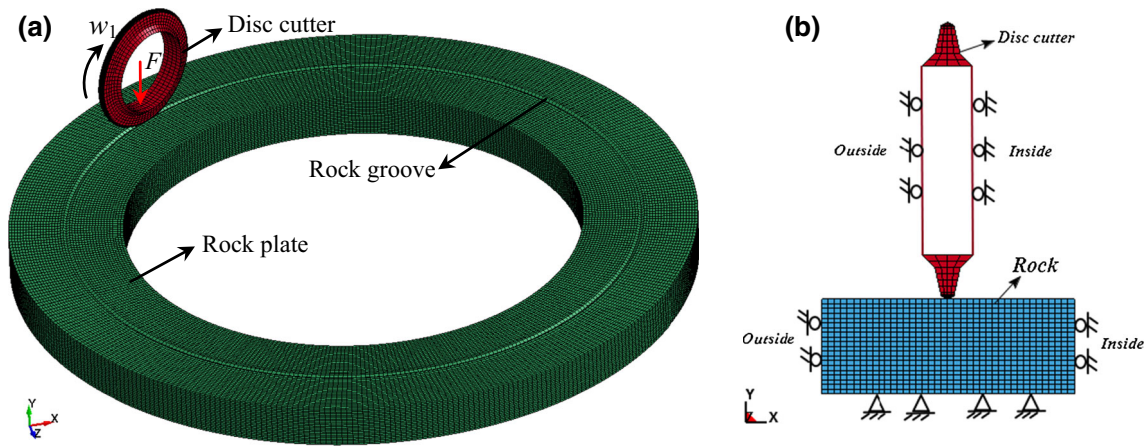


Fig. 2 Rock-breaking process of the disc cutter. **a** Finite element model. **b** Boundary conditions

temperature. In the tunneling process, it is important to reduce the disc cutter wear. Hence, abrasive wear is chosen as the most relevant type of wear for this analysis (Rad 1975).

3.1 Model for Predicting the Disc Cutter Wear Extent

The disc cutter wear is mainly caused by scratching between the quartz and other hard particles in rock and the tool surface. Therefore, to quantify abrasive wear through constitutive equations, the initial broken point of rock and the contact distance need to be determined. According to

Eqs. (22), (23), the bulk wear extent of the disc cutter can be expressed as

$$M = IW = \frac{\mu^2 \phi \pi R' N F_n I L}{V_0} \left(1 - \sqrt{1 - \frac{1}{\mu} \sqrt{\frac{p}{2R - p}}} \right) \quad (41)$$

Table 1 Material properties of the disc cutter

Parameters	Values
Density, ρ (kg/m ³)	8000
Young's modulus, E (GPa)	210
Poisson's ratio, ν	0.25
Friction coefficient, μ	0.23
Wear rate of energy, I (mm ³ /J)	5E-5

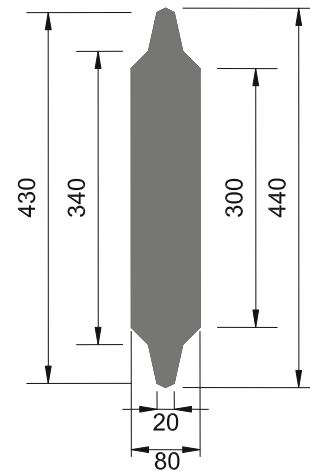


Fig. 3 Dimensions of disc cutter (unit: mm)

Table 2 Input parameters of the Johnson-Holmquist concrete model for rock (Holmquist and Johnson 1993)

Parameters	Values	Parameters	Values	Parameters	Values
Viscous constant, A	0.79	Enhancement coefficient, B	1.6	Coefficient of strain rate, C	0.007
Harding index, N	0.61	Maximum equivalent stress, S_{max}	7	Uniaxial compressive strength, f_c^c (MPa)	48
Elastic limit hydrostatic pressure, P_{crush} (MPa)	16	Volume strain corresponding to P_{crush} , μ_{crush}	0.001	Compaction hydrostatic pressure, P_{lock} (MPa)	800
Volume strain corresponding to P_{lock} , μ_{lock}	0.1	Maximum tensile hydrostatic stress, T (MPa)	2	Bulk modulus, K_1 (GPa)	85
Bulk modulus, K_2 (GPa)	-171	Bulk modulus, K_3 (GPa)	208	Damage constant, D_1	0.04
Damage constant, D_2	1	Shear modulus, G (GPa)	15	Minimum plastic strain, EF_{min}	0.01

where M is the disc cutter bulk wear extent, V_0 is the tunneling velocity of the cutter head, L is the total length of TBM tunneling, p is the penetration depth of the disc cutter, R' is the installing radius of the disc cutter, R is the radius of disc cutter, μ is the friction coefficient, N is the number of revolutions per minute of the TBM, F_n is the normal force acting on the disc cutter, ϕ is the angle of the theoretical contact arc, and μ is the friction coefficient between the cutting tool and rock. Additionally, I is the wear energy, which is also the bulk wear extent on the action of the frictional work under the specified

experimental condition. For a given rock mass and disc cutter material, I can be determined experimentally.

The wear of a cutting tool is a dynamic process and increases with the boring distance in TBM tunneling (Du and Gong 2012). This wear creates variation in the shape of the disc cutter. Therefore, Du and Gong (2012) put forward a model to estimate the cutter radial wear extent, which can be calculated as

$$M' = K_0 \cdot K_s \cdot \frac{L}{h} \cdot \frac{R}{r} \cdot l \tag{42}$$

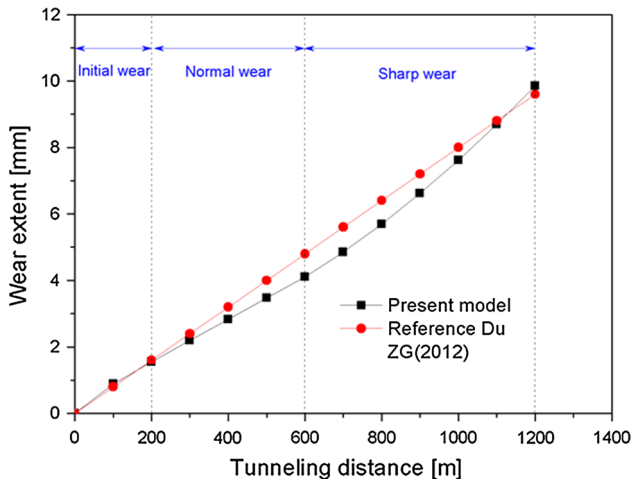


Fig. 4 Curve of disc cutter radial wear extent changes with tunneling distance

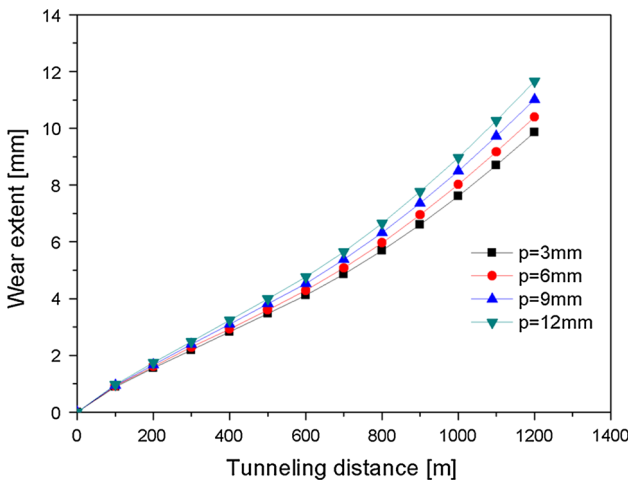


Fig. 5 Effect of cutting depth on the disc cutter wear extent. For using different penetration depth $p = 3, 6, 9$ and 12 mm to conduct four computational models, when keep the installing radius $R' = 1.0$ m and the vertical force acting on the disc cutter $F = 200$ kN

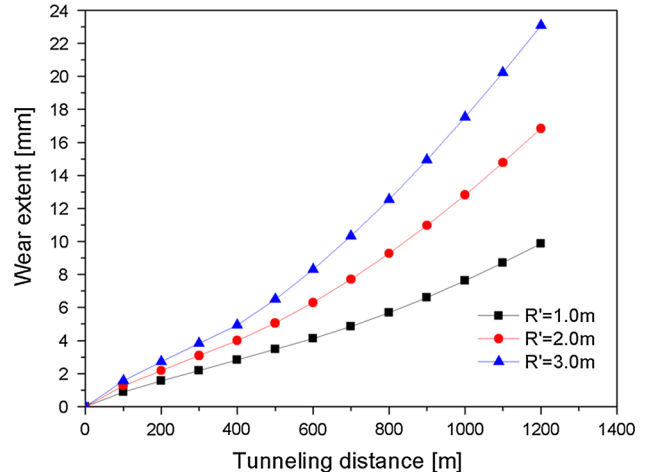


Fig. 6 Effect of installing radius on the disc cutter wear extent. For using different installing radius of the disc cutter $R' = 1.0, 2.0$ and 3.0 m to conduct three computational models, when keep the penetration depth $p = 3$ mm and the vertical force acting on the disc cutter $F = 200$ kN

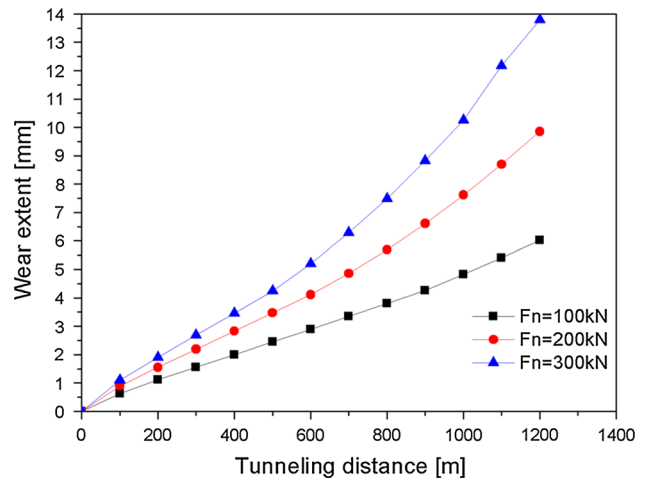


Fig. 7 Effect of the normal force on the disc cutter wear extent. For using different normal force acting on the rock $F_n = 100, 200$ and 300 kN to conduct three computational models, when keep the penetration depth $p = 3$ mm and the installing radius of the disc cutter $R' = 1.0$ m

where L is the total TBM tunneling length, h is the penetration, R is the disc cutter installing radius, r is the disc cutter radius, l is the arc length after the disc cutter has broken rock, and K_0 is the correction coefficient (greater than 1). K_0 and K_s can be obtained from experiments or practical construction experience, as proposed by Du and Gong (2012). K_0 is approximately 1.2–1.6 based on the construction experience for the Qinling tunnel. This value is usually determined by statistical or inverse analysis and is an empirical parameter.

3.2 Numerical Simulation of the Wear Extent of the Disc Cutter

For modeling, we employed a V-shaped disc cutter of 440 mm (17 in.) diameter and 80 mm thickness (as shown in Fig. 3), and the disc cutter installing radius was $R_i = 1.0$ m. As shown in Fig. 2, the rock plate inner radius, outer radius and thickness are $R_1 = 0.8$ m, $R_2 = 1.2$ m and $h_t = 0.15$ m, respectively. The above new model for wear was used in the disc cutter material model, and the input parameters for the cutter material model are summarized in Table 1. For the rock material model, we basically adopted the Johnson-Holmquist model (Johnson and Cook 1985),

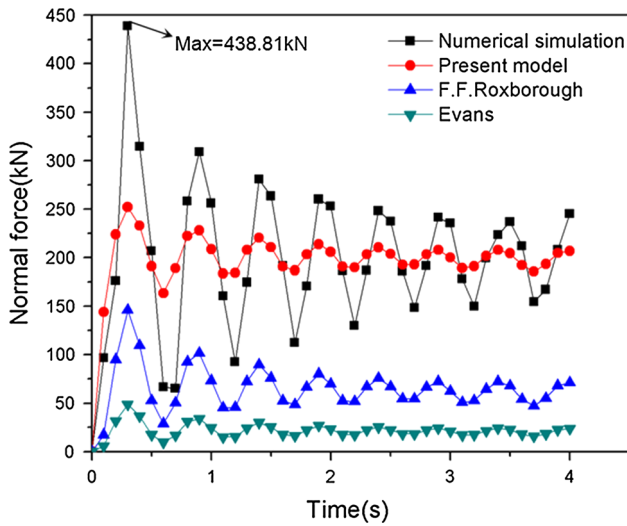


Fig. 8 The relationship between the normal force and the boring time when the wear extent of the disc cutter $w = 2.5$ mm

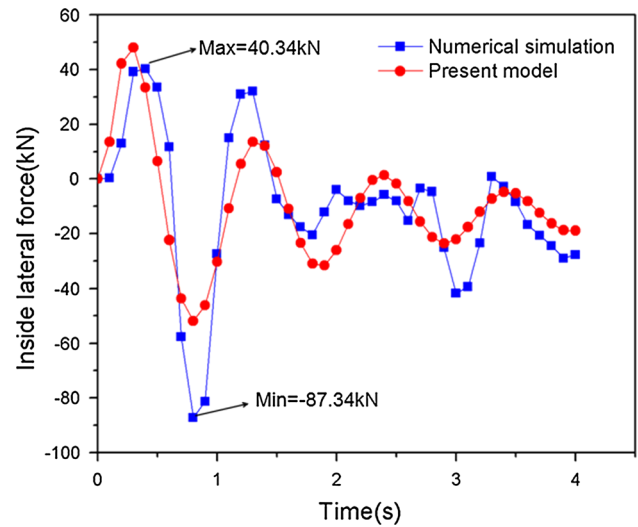


Fig. 10 The relationship between the internal lateral force and the boring time when the wear extent of the disc cutter $w = 2.5$ mm

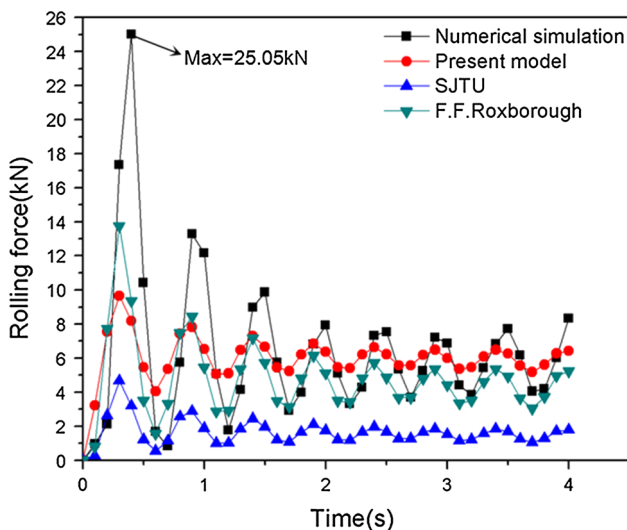


Fig. 9 The relationship between the rolling force and the boring time when the wear extent of the disc cutter $w = 2.5$ mm

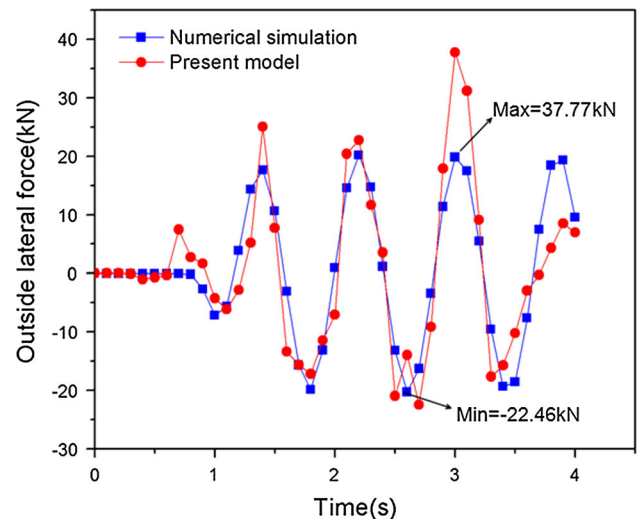


Fig. 11 The relationship between the outside lateral force and the boring time when the wear extent of the disc cutter $w = 2.5$ mm

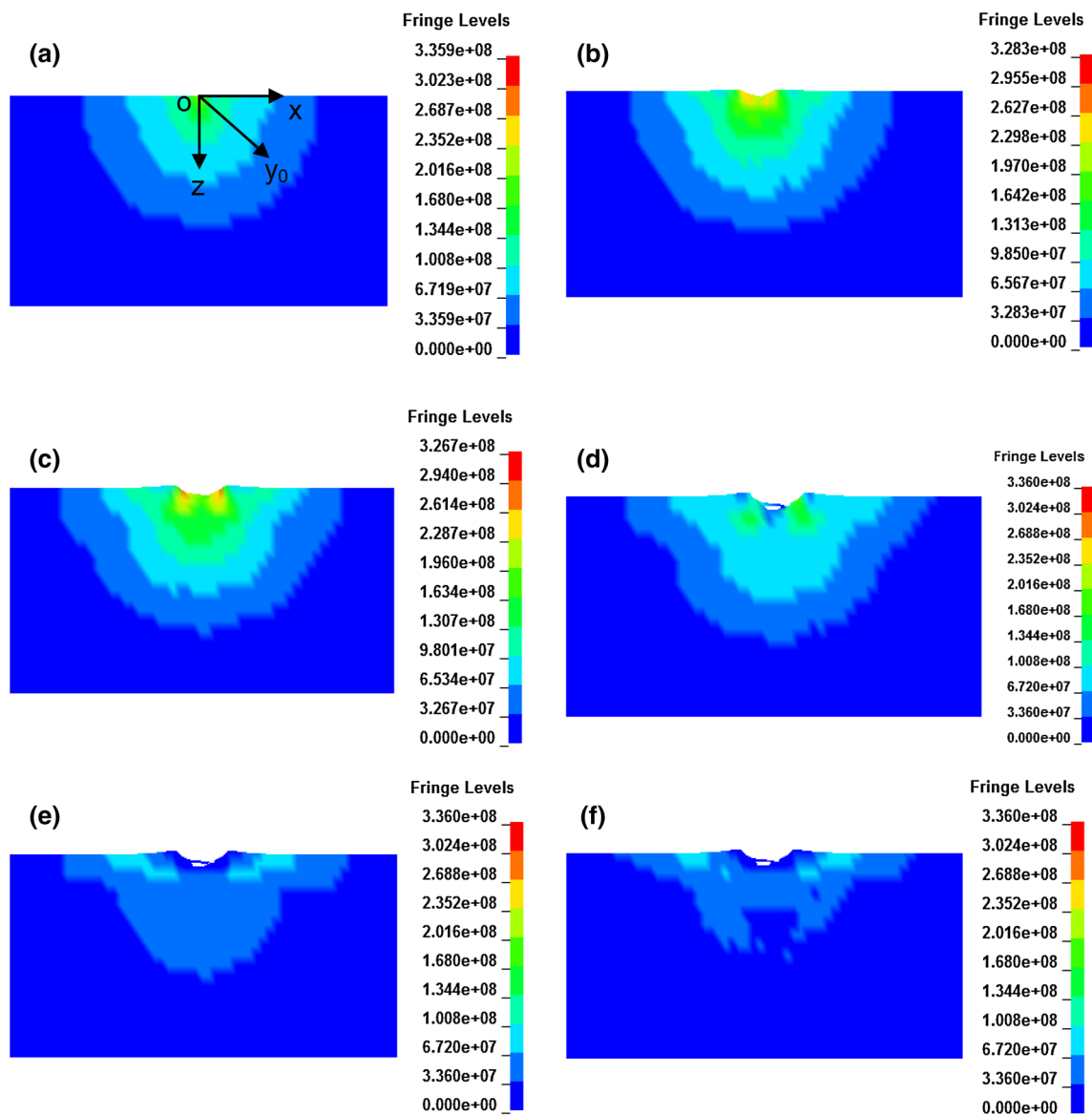


Fig. 12 Contour of rock’s Mises stress with different boring time and different penetration **a** $T = 0.85$ s, $p = 0.95$ mm; **b** $T = 0.9$ s, $p = 1.56$ mm; **c** $T = 0.95$ s, $p = 2.19$ mm; **d** $T = 1.0$ s, $p = 4.37$ mm; **e** $T = 1.05$ s, $p = 4.37$ mm; **f** $T = 1.1$ s, $p = 4.37$ mm

and the corresponding parameters are summarized by Holmquist and Johnson (1993) as shown in Table 2. The maximum tensile stress and maximum principal strain failure criteria were selected. The maximum tensile stress value is set to 2 MPa, and the maximum principal failure strain is 0.6. The vertical force acting on the disc cutter is $F = 200$ kN. The angular rotation and revolution velocities of the disc cutter are $w_1 = 1.5$ rad/s and $w_2 = 0.33$ rad/s, respectively. The disc cutter wear, rock-breaking process, and boundary conditions employed in the numerical model are shown in Fig. 2. In addition, to prevent unexpected failure induced by reflected stress waves, an infinite transmitting boundary condition (Century Dynamics Inc. 2003) was applied to each surface of the rock model except

for the upper surface. The disc cutter wear values estimated by the present model and the formula proposed by (Du and Gong 2012) are shown in Fig. 4.

Figure 4 indicates that the cutting tool wear generated in the boring process can generally be divided into three stages: initial wear, normal wear and sharp wear. In the initial wear stage, the disc cutter wear extent increases with time, and the slope of the curve increases gradually. As the slope of the curve ceases to change, the wear enters the normal wear stage, in which the wear increment is constant. The wear extent then enters the third wear stage, in which the wear extent increases sharply and the disc cutter must be replaced to ensure normal tunneling driving. The wear extents predicted by the present model and the model proposed by Du

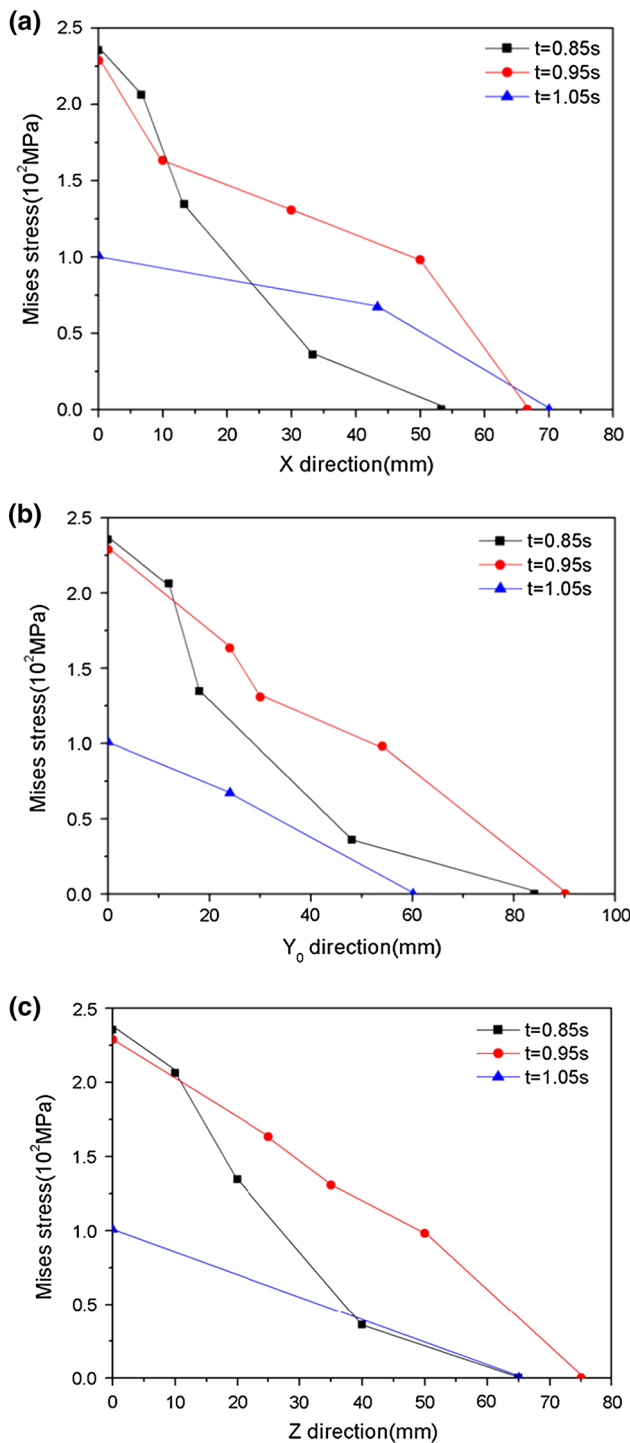


Fig. 13 Comparison of rock's Mises stress in different direction with different time: **a** in the X direction, **b** in the Y_0 direction and **c** in the Z direction

and Gong (2012) in Eq. (42) are compared in Fig. 4. It can be seen that the results obtained by the present model are slightly different from those obtained by Eq. (42).

To study the effect of penetration depth on the disc cutter wear, a series of calculations using different penetration

depths was conducted. The values of p were 3, 6, 9, and 12 mm, and the values of L ranged from 0 to 1200 m. As shown in Fig. 5, the change in the wear extent exhibits a similar trend for different values of p . The increment of the wear extent is rapid during the initial period of the boring process. The rate of increment then slows and approaches a constant value. Finally, the increment of wear extent increases again, approaching a new, higher constant value in the final stage. It can be further seen that the wear extent increases with increasing penetration depth for the same boring distance. As shown in Fig. 5, the tunneling distance L has a strong effect on the wear of the disc cutter, but the penetration p has a weak effect on the disc cutter wear.

A series of calculations was conducted using different installing radii to assess the effect of installing radius R' on the disc cutter wear extent. The values of R' were 1.0, 2.0, and 3.0 m, and the range of L was 0–1200 m. As shown in Fig. 6, the change in the wear extent exhibits a similar trend for different values of R' . The increment of the wear extent is large in the initial period of the boring process. The increment of wear extent then slows and remains basically unchanged. Finally, the increment of wear extent increases again and approaches a new, higher constant value in the final stage. It can also be seen that the wear extent increases with increasing installing radius for the same boring distance. As shown in Fig. 6, the distance between the center of the cutter head and the disc cutter R' has a strong effect on the disc cutter wear.

We conducted a series of calculations using different normal forces acting on the disc cutter to investigate the effect of the normal force F_n on the disc cutter wear extent. The values of F_n were 100, 200, and 300 kN, and the range of L was 0–1200 m. As shown in Fig. 7, the change in the wear extent exhibited a similar trend for different values of F_n . The increment of the wear extent is large in the initial period of the boring process. The increment of the wear extent then slows and remains basically unchanged. Finally, the increment of the wear extent increases again and approaches a new, higher constant value in the final stage. It can be further seen that the wear extent increases with the normal force acting on the disc cutter for the same boring distance. Therefore, the normal force acting on the disc cutter F_n has a strong effect on the wear of the disc cutter.

4 Numerical Simulation of the Rock Damage Process During Tunneling

The excavation of a massive rock by a boring machine is usually analyzed by studying a single cutting tool. Characteristic tools are commonly studied via laboratory tests. According to the obtained results, analytical formulas are

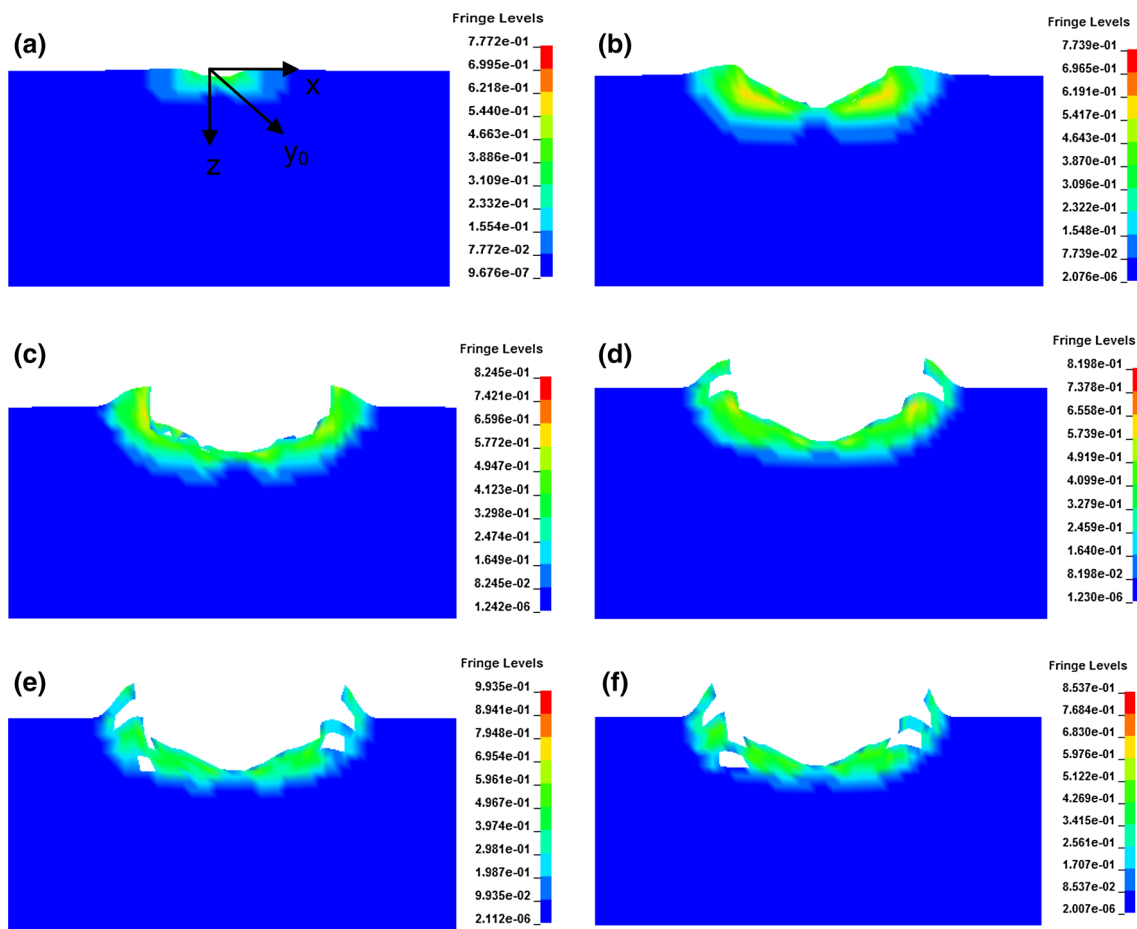


Fig. 14 Contour of rock's Mises strain with different boring time and different penetration **a** $T = 0.85$ s, $p = 0.95$ mm; **b** $T = 0.9$ s, $p = 1.56$ mm; **c** $T = 0.95$ s, $p = 2.19$ mm; **d** $T = 1.0$ s, $p = 4.37$ mm; **e** $T = 1.05$ s, $p = 4.37$ mm; **f** $T = 1.1$ s, $p = 4.37$ mm

applied to determine the parameters that describe the behavior of the entire tunneling machine. This type of study mainly relies on the tunneling experience of analysts and experimental testing.

The numerical simulation of excavation is a relatively new approach resulting from a breakthrough in the development of new computational mechanics techniques. In most numerical simulations of rock breakage by disc cutters (Liu et al. 2002; Kou et al. 2004), the running path of the disc cutter is linear. However, we know that the actual moving path of the disc cutter is circular. Additionally, many researchers (Liu et al. 2002; Kou et al. 2004) have analyzed the cutting force without considering disc cutter wear, which may affect the cutting force. Thus, we focused on the two issues above when conducting the numerical simulations.

4.1 Validity of the Prediction Formula for Cutting Force

The relevant parameters are assumed as follows. A V-shaped disc cutter of 440 mm (17 in.) in diameter and 80 mm in

thickness is employed. The disc cutter installing radius is $R_i = 1.0$ m, and the inner radius, outer radius, and thickness of the rock plate are $R_1 = 0.8$ m, $R_2 = 1.2$ m, and $h_t = 0.15$ m, respectively. The vertical force acting on the disc cutter is $F = 200$ kN. The angular rotation and revolution velocities of the disc cutter are $w_1 = 1.5$ rad/s and $w_2 = 0.33$ rad/s, respectively. The radial wear extent of the disc cutter is $w = 2.5$ mm, the path correction coefficients are $k_{np} = 1.01$ and $k_{rp} = 0.433$, and the wear correction coefficients are $k_{nw} = 1.58e^{-6}$ and $k_{rw} = 6.74e^{-5}$. The rigid model from the ANSYS/LS-DYNA library was used for the disc cutter material model, and the input parameters for the cutter material model can be found in Table 1. For the rock material model, we basically adopted the Johnson-Holmquist concrete model (Johnson and Cook 1985) and the corresponding parameters in ANSYS/LS-DYNA summarized by Holmquist and Johnson (1993), as shown in Table 2. The rock plate is simulated using finite element meshes, namely, elements in ANSYS/LS-DYNA. The disc cutter and rock employed the element SOLID 164 in the computational model, and the element size of the rock is 5 mm.

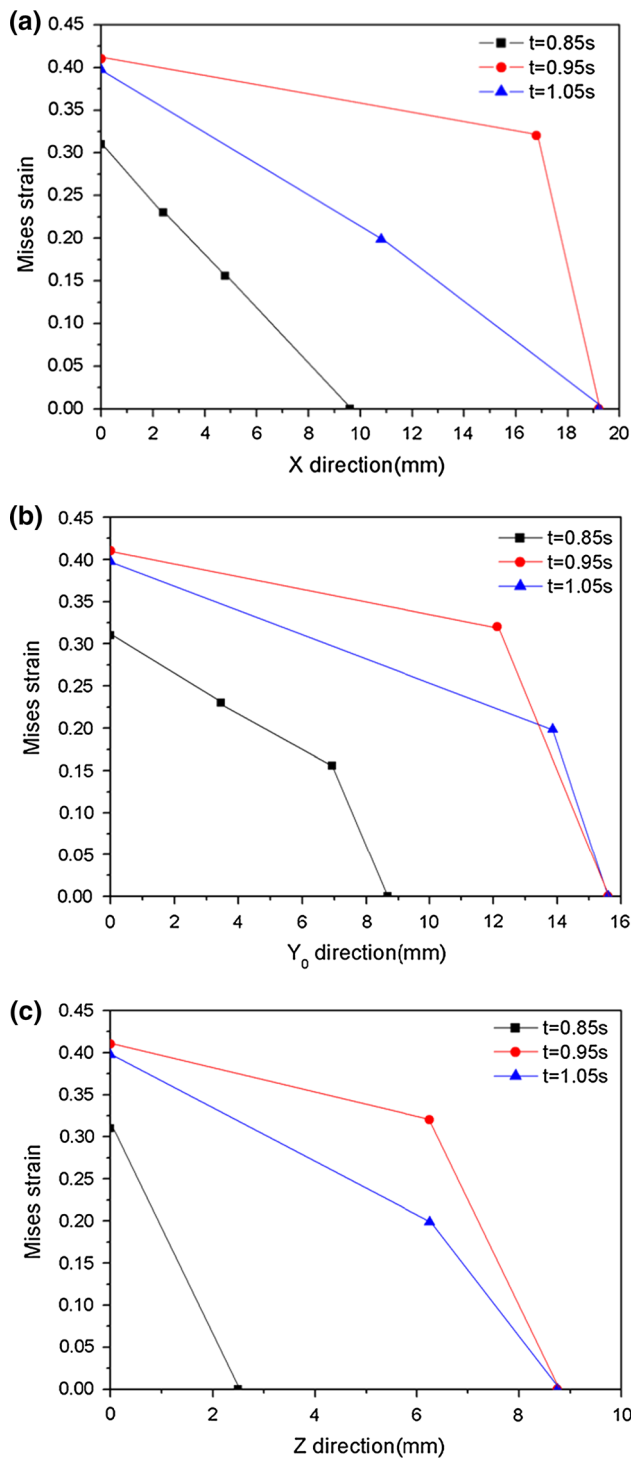


Fig. 15 Comparison of rock's Mises strain in different direction with different time **a** in the X direction, **b** in the Y_0 direction and **c** in the Z direction

We employed the *CONTACT_ERODING_SURFACE_TO_SURFACE algorithm from the LS_DYNA library to simulate the contact between the disc cutter and the rock. The contact algorithm is a penetration contact algorithm. When material failure occurs in the contact process, contact can still

occur for the remaining elements, which is mainly used for the solid element surface penetration failure problem. In the rock-breaking process, the failure of rock is highly nonlinear, making the contact algorithm appropriate. In the definition of contact, the disc cutter is regarded as the contact surface, and the rock is regarded as the target surface. The contact static friction coefficient is defined as 0.4, and the dynamic friction coefficient is defined as 0.35. The material failure criteria of the maximum tensile stress and the maximum principal strain failure criteria were selected. The maximum tensile stress is 2 MPa, and the maximum principal strain failure is 0.6. The disc cutter wear, rock-breaking process, and the boundary conditions employed in the numerical model are shown in Fig. 2. In addition, an infinite transmitting boundary condition (Century Dynamics Inc. 2003) was applied to the rock model surfaces, except for the upper surface, to prevent unexpected failure induced by reflected stress waves and exclude the scale effect associated with the finite dimensions of the rock model. The predicted cutting forces of the disc cutter obtained by the numerical simulation, the present model and the existing formulas are shown in Figs. 8, 9, 10, 11, allowing the accuracy of the prediction formula proposed in this paper to be verified.

The cutting forces acting on the rock generated by a single disc cutter with a certain wear extent are shown in Figs. 8, 9, 10, 11. It can be seen that the cutting forces are not constant and instead fluctuate around an average value, which is consistent with the stress status in the actual rock breakage process. This phenomenon may be caused by the brittle property of the rock material. In Fig. 8, the mean value of the normal force is 197.86 kN, and the maximum value of the normal force is 438.81 kN. In Fig. 9, the mean value of the rolling force is 6.33 kN, the maximum value of the rolling force is 25.02 kN. According to the numerical simulation results, the normal force is much greater than the rolling force.

The normal forces obtained using the present prediction model, the numerical simulation and the existing formulas proposed by Roxborough and Phillips (1975) and (Evans and Pomeroy 1966) are compared. The existing formulas proposed by Roxborough and Phillips (1975) and Evans and Pomeroy (1966) are as follows, respectively:

$$F_V^R = 4\sigma_c h \tan \alpha \sqrt{2Rh - h^2} \quad (43)$$

$$F_V^E = \frac{4}{3} \sigma_c h \sqrt{R^2 - (R - h)^2} \tan \alpha \quad (44)$$

where F_V is the normal force, σ_c is the rock uniaxial compressive strength, α is the edge angle of the disc cutter, R is the radius of the disc cutter, and h is the penetration depth of the disc cutter.

As shown in Fig. 8, regardless of whether the values are obtained by the present model or by Eq. (43) proposed by Roxborough and Phillips (1975) and Eq. (44) proposed by

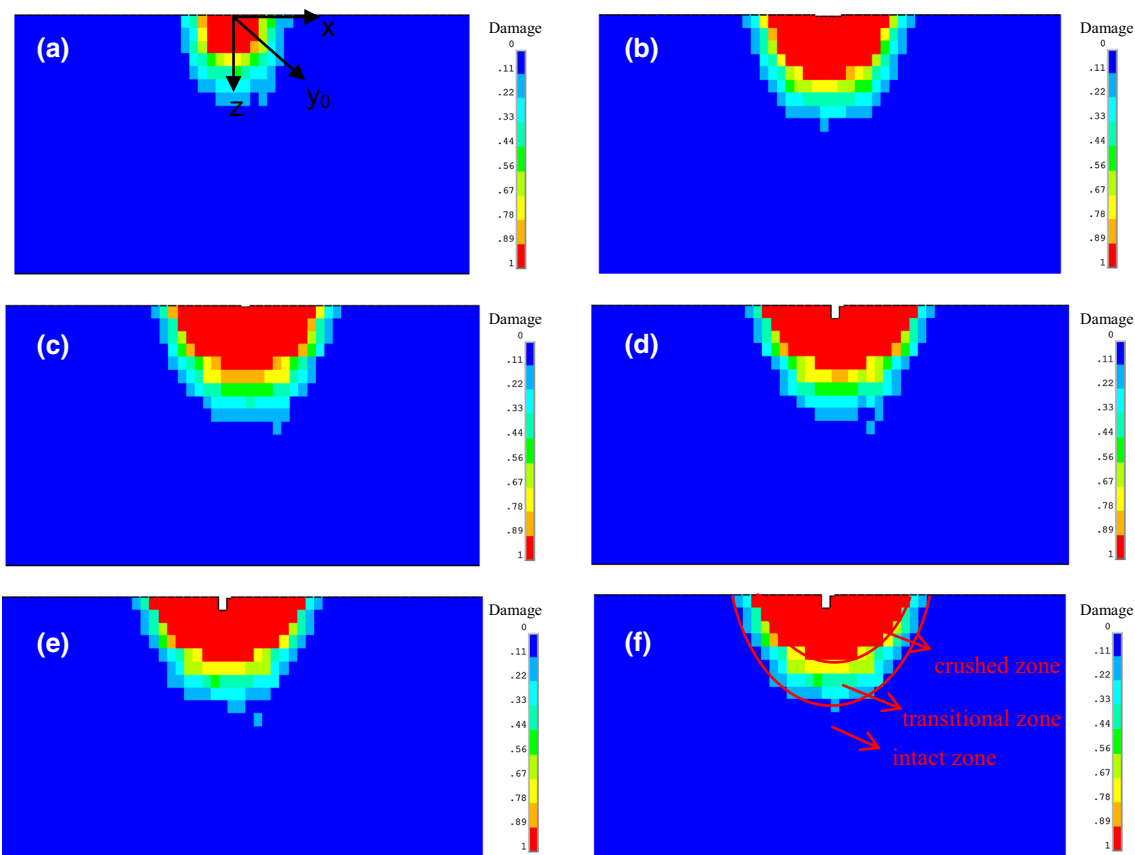


Fig. 16 Contour of rock’s damage with different boring time and different penetration **a** $T = 0.85$ s, $p = 0.95$ mm; **b** $T = 0.9$ s, $p = 1.56$ mm; **c** $T = 0.95$ s, $p = 2.19$ mm; **d** $T = 1.0$ s, $p = 4.37$ mm; **e** $T = 1.05$ s, $p = 4.37$ mm; **f** $T = 1.1$ s, $p = 4.37$ mm

Evans and Pomeroy (1966), the variation in the normal force with increasing boring time exhibits a similar trend. It also can be seen from Fig. 8 that the results obtained with the present model differ slightly from those obtained by Eqs. (43) and (44). Specifically, the normal force obtained with the present model is larger than that estimated by Eqs. (43) and (44), which does not consider the effects of the disc cutter’s operating path and the disc cutter wear on the normal force. Therefore, the circular running path and the disc cutter wear may affect the normal force of the disc cutter.

Fig 9 compares the results of the rolling force acting on the disc cutter obtained by the present model and existing formulas proposed by Roxborough and Phillips (1975) and SJTU (Zhang 2008). The existing formulas proposed by Roxborough and Phillips (1975) and SJTU (Zhang 2008) are as follows, respectively:

$$F_R = 4\sigma_c h^2 \tan \alpha \tag{45}$$

$$F_R = F_V \left(\sqrt{\frac{h}{D} + \mu \frac{d}{D}} \right) \tag{46}$$

where F_R is the rolling force, F_V is the normal force, α is the edge angle of the disc cutter, h is the penetration depth of the disc cutter, μ is the friction coefficient (0.02 in this paper), D is the diameter of the disc cutter ring, and d is the diameter of the disc cutter shaft.

As shown in Fig. 9, regardless of whether the values are obtained by the present model by Eq. (45) proposed by Roxborough and Phillips (1975) and Eq. (46) proposed by SJTU (Zhang 2008), the change in the rolling force with increasing boring time exhibits a similar trend. It also can be seen in Fig. 9 that the results obtained with the present model are highly consistent with those obtained with Eq. (45), and the normal force obtained with the present model is larger than that estimated by Eq. (46). Therefore, the circular running path and the disc cutter wear may also affect the rolling force of the disc cutter.

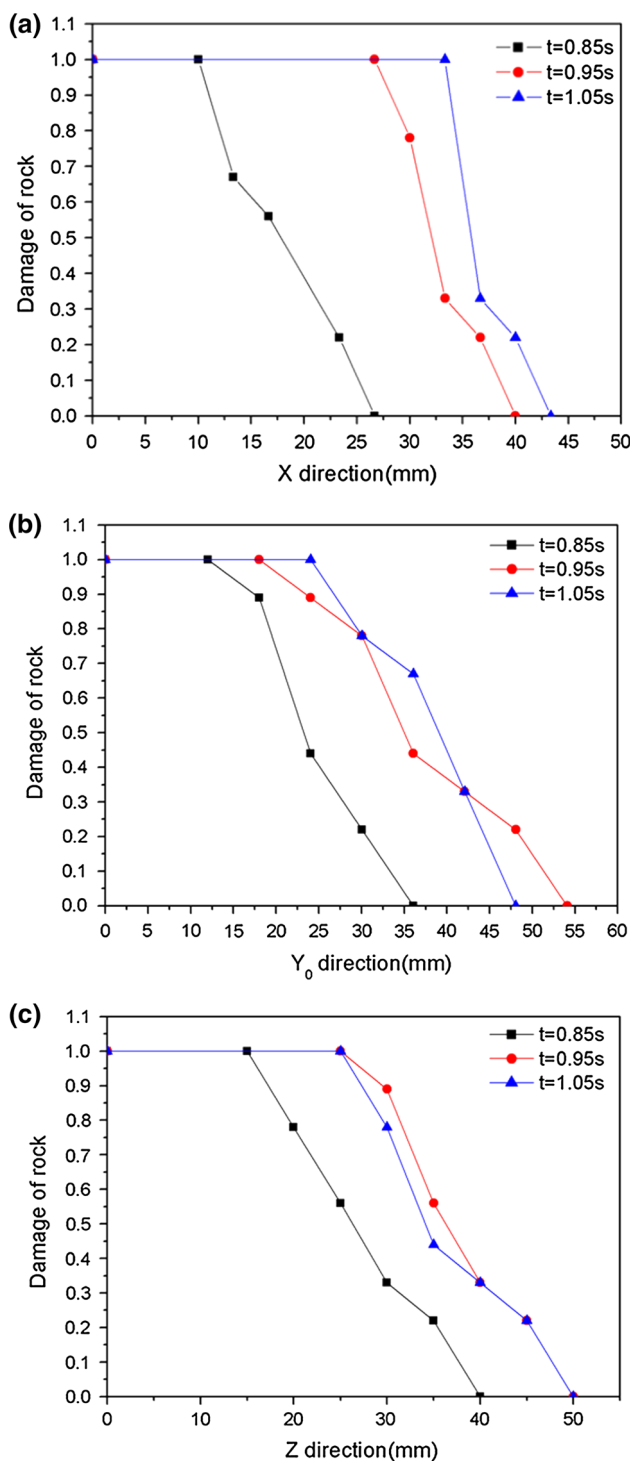


Fig. 17 Comparison of rock's damage in different direction with different time **a** in the X direction, **b** in the Y_0 direction and **c** in the Z direction

It can be seen from Figs. 10, 11 that the change in the internal or external lateral force, with boring time is similar regardless of whether the values were obtained by the numerical simulation or the present model. Figures 10 and

11 also indicate that the maximum and minimum values of the internal lateral force are 40.34 and -87.34 kN, respectively, and the maximum and minimum values of the external lateral force are 37.77 and -22.46 kN, respectively. Thus, the internal lateral force varies to a greater extent than the external lateral force. It is obvious that the internal lateral force is larger than the external lateral force, and this phenomenon is significant in the initial rock breakage stage.

For a constant disc cutter driving speed, the increase in the contact area between the disc cutter and rock upon increasing wear gradually increases the cutting force. Thus, in actual engineering applications (Yin et al. 2014), to keep the tunneling speed constant, we must increase the thrust of the hydraulic jack. According to the analysis above, the simulation results are consistent with this.

4.2 Analysis of Rock Breakage Process Under Different Penetration Condition

As the disc cutter breaks rock, the tip of disc cutter makes contact with the rock and then induces the elastic deformation of the rock in the initial stage. As the penetration depth increases, the plastic deformation of rock occurs, leading to damage accumulation in the rock. When the rock is completely damaged, rock breakage occurs.

We cut the rock in a plane to observe the inner rock breakage at $T = 0.95$ s. The contours of the von Mises stress and strain of the rock for different boring times and penetration depths are shown in Figs. 12, 14, respectively, and the damage field of the rock is presented in Fig. 16, where the time steps were $T = 0.85\text{--}1.1$ s. Figures 12 and 14 show the rock failure during the disc cutter rock breakage process. The rock groove width is greater than the tip width, which may be due to the brittleness of the rock material, and the penetration depth of the disc cutter increases with the boring time. The von Mises stress values of the rock in the X , Y_0 and Z directions over time are compared in Fig. 13. The von Mises stress of the rock decreases with the values of X , Y_0 and Z , and the cutting of the disc cutter into the rock makes the extrusion stress increase gradually. When the stress reaches the yield strength, the plastic deformation of the rock occurred, followed by rock breakage, a decrease in extrusion stress, and then the process cycle. Therefore, in the process of disc cutter rock breakage, the rock constantly experiences loading and unloading; thus, the rock breaking is a sudden failure process, as shown in Figs. 13, 15.

The rock under the action of a single TBM disc cutter can be divided into three zones, namely, the crushed zone, the transitional zone and the intact zone, as shown in Fig. 16.

The rock damage in the X , Y_0 and Z directions over time is shown in Fig. 17. It can be seen that the rock damage decreases as X , Y_0 and Z increase, and the damage field of the rock increases over time.

5 Conclusions

A model for estimating the cutting force on the disc cutter in tunneling process is developed by considering the circular running path and wear of the disc cutter. This method can be applied to improve the TBM penetration design. The cutting force on the rock generated by a single disc cutter is simulated by using the explicit dynamic finite element method ANSYS/LS_DYNA, and the rock breakage is discussed. The simulation results are analyzed and compared with the cutting force prediction model and the estimation formula proposed by Roxborough, Evans and SJTU (Roxborough and Phillips 1975; Zhang 2008). Moreover, a quantitative slip theory for rolling contact considering the effect of tangential traction is also introduced based on contact mechanics. An evaluation model including the disc cutter parameters and boring parameters is also discussed to estimate the wear extent of the disc cutter.

It is shown that the wear extent increases with the penetration depth for a given boring distance. The wear extent also increases with increasing installing radius and increasing normal force acting on the disc cutter. Thus, the disc cutter parameters and boring parameters have a strong effect on the wear of the disc cutter. A comparison of the validity of the prediction models shows that the cutting force prediction model presented in this study is superior to the other models. Therefore, this prediction model can be used to provide guidance for TBM design and application in tunnel excavation.

Although the effect of the dynamic response of the rock breakage on the cutting force has not yet been considered research to introduce this behavior into the present prediction model is underway. The model proposed in this paper does not consider changes of rock damage and mechanical parameters near disk cutter. Moreover, a new cutting force prediction model considering mixed ground conditions should also be developed.

Acknowledgments The financial support of the Fundamental Research Funds for the Central Universities (Project Nos. CDJZR200013), general project of Chongqing Foundation (cstc2014-jcyjA30016), the Research Fund of the Key Laboratory of Tunneling Engineering at Southwestern Jiaotong University (TTE2014-04), the National Basic Research Program of China (973 Program, No. 2014CB046903) and the Natural Science Fund of China (No. 51409026) is greatly appreciated.

References

- An M, Yu MH, Wu X (1991) Generalized twin shear stress yield criterion in rock mechanics. *Rock Soil Mech* 12(1):17–26
- Baek SH, Moon HK (2003) A numerical study on the rock fragmentation by TBM cutter penetration. *Tunn Undergr Space (J Korean Soc Rock Mech)* 13(6):444–454
- Bilgin N, Tuncdemir H, Balci C, Copur H, Eskikaya S (2000) A model to predict the performance of tunneling machines under stressed conditions. In: *Proceedings, AITES-ITA 2000 World Tunnel Congress*, pp 47–53
- Century Dynamics Inc (2003) AUTODYN theory manual. Century Dynamics Inc, Concord
- Chiaia B (2001) Fracture mechanisms induced in a brittle material by a hard cutting indenter. *Int J Solids Struct* 38:7747–7768
- Cigla M, Yagiz S, Ozdemir L (2001) Application of Tunnel Boring Machines in Underground Mine Development. In: *17th International Mining Congress and Exhibition of Turkey*. Turkey, pp 155–164
- Cook NGW, Hood M, Tsai F (1984) Observations of crack growth in hard rock loaded by an indenter. *Int J Rock Mech Min Sci Geomech Abstr* 21(2):97–107
- Du ZG, Gong YD (2012) Research on the wear of TBM disc cutters based on the arc of the rock breakage. *Constr Mach* 5:73–76
- Eoxborough FF, Philips HR (1975) The mechanical properties and cutting characteristics of the Bunter Sandstone. Report to TRRL, University of Newcastle upon Tyne, pp 292
- Evans I, Pomeroy CD (1966) The strength, fracture and workability of coal. Pergamon, London, p 277
- Gong QM, Zhao J (2005) Numerical modeling of the effects of joint orientation on rock fragmentation by TBM cutters. *Tunn Undergr Sp Technol* 20(2):183–191
- Gong QM, Zhao J, Jiao YY (2006) Numerical modeling of the effects of joint spacing on rock fragmentation by TBM cutters. *Tunn Undergr Sp Technol* 21(1):46–55
- Goryacheva IG, Goryachev AP (2006) The wear contact problem with partial slippage. *Appl Mech Mater* 70:934–944
- Holmquist TJ, Johnson GR (1993) A computational constitutive model for concrete subjected to large strain, high strain rates, and high pressures, In: *Proceedings of the 14th International Symposium on Ballistics, Quebec*, pp 591–600
- Johnson GR, Cook WH (1985) Fracture characteristics of three metals subjected to various strains, strain rates, temperatures and pressures. *Eng Fract Mech* 21(1):31–48
- Kou SQ, Liu HY, Lindqvist PA, Tang CA (2004) Rock fragmentation mechanisms induced by a drill bit. *Int J Rock Mech Min Sci* 41(3):460
- Li FH, Zhong XC, Yi LK (2011) A theoretical model for estimating the wear of the disc cutter. *Appl Mech Mater* 90:2232–2236
- Li SJ, Feng XT, Li ZH, Zhang CQ, Chen BR (2012) Evolution of fractures in the excavation damaged zone of a deeply buried tunnel during TBM construction. *Int J Rock Mech Min Sci* 55(10):125–138
- Li SJ, Feng XT, Wang CY, Hudson JA (2013) ISRM suggested method for rock fractures observations using a borehole digital optical televiewer. *Rock Mech Rock Eng* 46:635–644
- Liu C (2003) Development on disc cutter-key component of TBM. *Chin Railway Sci* 24(4):101–106
- Liu HY, Kou SQ, Lindqvist CA (2002) A numerical simulation of the rock fragmentation process induced by indenters. *Int J Rock Mech Min Sci* 39:491–505
- Liu QS, Shi K, Zhu YG, Huang X (2013) Calculation model for rock disc cutter forces of TBM. *Chin Coal Sci* 38(7):1136–1142
- Pang SS, Goldsmith W (1990) Investigation of crack formation during loading of brittle rock. *Rock Mech Rock Eng* 23:53–63

- Paul B, Sikarskie DL (1965) A preliminary theory of static penetration of a rigid wedge into a brittle material. *Trans Soc Min Eng AIME* 232:372–383
- Rad PF (1975) Bluntness and wear of rolling disk cutters. *Int J Rock Mech Min Sci Geomech Abstr* 12:93–99
- Rostami J, Ozdemir L, Nilsen B (1996) Comparison between CSM and NTH hard rock TBM performance prediction models. In: *Proceedings of Annual Technical Meeting of the Institute of Shaft Drilling and Technology (ISDT)*, Las Vegas, NV, p 11
- Roxborough FF, Phillips HR (1975) Rock excavation by disc cutter. *Int J Rock Mech Min Sci Geomech Abstr* 12(12):361–366
- Su PC, Wang WS, Huo JH (2010) Optimal layout design of cutters on tunnel boring machine. *J Northeastern Univ* 31:877–881
- Tohson KL (1989) *Contact mechanics*. Cambridge University Publishers, London
- Wan ZC, Sha MY, Zhou YL (2002) Study on disc cutters for hard rock application of TB880E TBM in Qinling tunnel (2). *Modern tunn Technol* 39(6):1–12
- Yin LJ, Gong QM, Zhao J (2014) Study on rock mass boreability by TBM penetration test under different in situ stress conditions. *Tunn Undergr Space Technol* 43:413–425
- Yu TQ, Qian JC (1990) *Damage theory and its application*. National Defence Industry Press, Beijing
- Zhang HM (2006) The method to estimate cutter wear of tunnel boring machine. In: Chinese: CN1818640, 16th, August
- Zhang ZH (2008) The research on theory and techniques of service life management of TBM disc cutters. PhD thesis, North China Electric Power University, China
- Zhang ZH, Ji CM (2009) Analytic solution and its usage of arc length of rock breakage point of disc edge on full face rock tunnel boring machine. *J Basic Sci Eng* 17(2):265–273
- Zhang L, Lu GH (2010) Damage evolution model for rocks based on strain states. *J Hohai Univ* 38(2):176–180
- Zhao WG, Liu MY, Du YL (2007) Abnormal cutter wear recognition of full face tunnel boring machine (TBM). *Chin Mech Eng* 18(2):150–153